

## Experimental and FEM analysis of mar behavior on amorphous polymers

Du, Shuoran; Hamdi, Marouen; Sue, Hung Jue

**DOI**

[10.1016/j.wear.2019.203155](https://doi.org/10.1016/j.wear.2019.203155)

**Publication date**

2020

**Document Version**

Accepted author manuscript

**Published in**

Wear

**Citation (APA)**

Du, S., Hamdi, M., & Sue, H. J. (2020). Experimental and FEM analysis of mar behavior on amorphous polymers. *Wear*, 444-445, Article 203155. <https://doi.org/10.1016/j.wear.2019.203155>

**Important note**

To cite this publication, please use the final published version (if applicable).  
Please check the document version above.

**Copyright**

Other than for strictly personal use, it is not permitted to download, forward or distribute the text or part of it, without the consent of the author(s) and/or copyright holder(s), unless the work is under an open content license such as Creative Commons.

**Takedown policy**

Please contact us and provide details if you believe this document breaches copyrights.  
We will remove access to the work immediately and investigate your claim.

# EXPERIMENTAL AND FEM ANALYSIS OF MAR BEHAVIOR ON AMORPHOUS POLYMERS.

Shuoran Du<sup>a</sup>, Marouen Hamdi<sup>b</sup>, and Hung-Jue Sue<sup>c</sup>

<sup>a</sup> *J. Mike Walker '66 Department of Mechanical Engineering, Polymer Technology Center, Texas A&M University, College Station, TX 77843, USA*

<sup>b</sup> *Faculty of Aerospace Engineering, Department of Aerospace Structures and Materials, Group of Structural Integrity and Composites, Delft University of Technology, Kluyverweg 3, 2629 HS Delft, The Netherlands*

<sup>c</sup> *Department of Materials Science and Engineering, Polymer Technology Center, Texas A&M University, College Station, TX 77843, USA*

\* *Corresponding author. E-mail address: hjsue@tamu.edu (H.-J. Sue)*

## Abstract

Mar is a type of subtle surface damage caused by a sliding object barely visible to human eyes. This minor damage phenomenon has rarely been systematically studied. Significant research efforts for the fundamental understanding of mar behavior in polymers are still needed. In this study, the mar behavior of a series of model amorphous polymers, i.e., polymethylmethacrylate (PMMA), polycarbonate (PC), and polystyrene (PS), were investigated based on a modified ASTM/ISO scratch testing methodology and a corresponding finite element method (FEM) modeling. Furthermore, the mar-induced visibility and material parameter relationships were established through a systematic FEM parametric study. Experimental results show that PMMA has the highest mar visibility resistance, indicated by lower surface roughness variation and low contrast between marred region and the background. The numerical analysis showed that the maximum plastic principal strain ( $\epsilon_1^p$ ) and total dissipated plastic energy ( $E_p$ ) can be considered for evaluating mar visibility resistance. Higher mar visibility resistance corresponds to lower  $\epsilon_1^p$  and  $E_p$  values. Based on these two criteria, the parametric analysis shows that mar visibility resistance increases with lower modulus, higher yield stress, higher hardening slope, and lower softening slope. The usefulness of the present study for the preparation of mar resistant polymers is discussed.

**Keywords:** surface damage; mar performance; finite element method; parametric analysis; amorphous polymers.

## I. INTRODUCTION

Retention of the surface properties of polymeric materials is a significant indicator of the quality of many products such as cellular phone casings, packages, and automotive components. Thanks to large volumes of research activities in recent years, single path tribological polymer surface damage features have been well recognized and categorized as ‘scratch’ and ‘mar’[1-4]. Scratch is a significant surface deformation caused by sliding a sharp asperity. Mar is a subtle surface damage caused by sliding objects on the material surface barely visible to human eyes.

Previous studies quantified scratch resistance based on the scratch groove dimensions, namely its depth, width, and shoulder height [5-8]. Furthermore, distinctive damage transitions are commonly observed along the scratch path as the applied scratch load increases according to the ASTM-7027/ISO-19252 standards. For example, Browning found that periodic micro-cracks developed in the scratch groove for brittle styrene-acrylonitrile (SAN) random copolymers when the scratch normal load reached a critical value [9]. For higher scratch loads, continuous plowing with massive material removal is observed. For ductile polymers, periodic fish-scale type damage dominated by stick-slip phenomenon was observed [10, 11]. These scratch behaviors were not observed in the case of mar damage. Unlike scratch, this subtle damage feature cannot be easily quantified because of the gradual evolution of mar damage severity upon increased loading. Also, no clear damage transitions could be observed on the mar path. Instead, only progressive changes in surface roughness and possible wavy or proto-craze types of surface damages were found [12]. This makes mar quantification and analysis considerably challenging.

Mar damage can be caused by one or a combination of the following mechanisms: meniscus wrinkling, uneven viscoelastic deformation, localized molecular orientation, crazing, shear banding, and micro-cracking. The underlying physics of most of these mechanisms are still unclear and cannot be easily modeled. Depending on the surface properties, mar damage can be induced by ironing or roughening mechanisms [13]. Ironing process is usually formed on rough surfaces. Surface asperities are suppressed by the smoother mar tip and the mar area becomes smoother than the background of the sample. In contrast, roughening mar is usually formed on smooth surfaces. The damaged area is roughened by the mar tip.

Mar tests on polymer surfaces were performed using either a smooth barrel head or a rough sandpaper surface [1]. A smooth barrel head usually causes ironing mar. However, it can also induce roughening damage when the tip roughness of the mar head is higher than that of the polymer surface [13]. Given its significant roughness, the sandpaper surface can only generate roughening mar damage. Recently, the smooth barrel tip was used to conduct mar tests on textured thermoplastic olefin (TPO) used for automotive interior parts. This study found a good correlation between the obtained mar damage performance and the results of initial quality surveys (IQS) filled out by consumers [14]. Therefore, this testing condition will be considered in our study because of its simplicity and practicality.

Limited studies were conducted to investigate the behavior of mar damage [8, 13]. A fundamental understanding of how the constitutive behavior influences the mar resistance is needed. Previous research has shown that finite element methods (FEM) modeling is effectively

in investigating the effect of polymer constitutive parameters on scratch behavior [15-18]. The same methodology was also used to quantitatively predict scratch damage features in ductile amorphous polymers [16]. FEM modeling has been shown to be an efficient research tool for understanding the surface deformation and damage in polymers. In this study, a similar FEM approach was chosen to investigate mar behavior. Given that mar damage feature dimensions are considerably low and cannot be used as a quantification parameter, other alternative criteria should be explored to correlate between mar performance and material parameters. For simplicity, only the elastic-plastic smooth surfaces without asperities will be considered for the present FEM mar behavior simulation.

Also, since it is extremely difficult to experimentally choose polymers with systematic change in their constitutive property without altering other properties, a parametric analysis will be performed to separately determine the impact of the constitutive properties on mar behavior. For instance, previous studies showed that the elastic modulus and yield stress are usually coupled [19-21]. Similarly, the softening and hardening slopes are interconnected as in the case of PS modified with poly(2,6-dimethyl-1,4-phenylene oxide) or di-(ethyl glycol)-dimethacrylate cross-linking agent [22]. Therefore, parametric studies will be conducted using FEM modeling.

The main objectives of the present research are twofold: (1) establish the correlation between the mar behavior and the material's constitutive properties and (2) propose useful criteria for the quantitative assessment of mar performance. For experimental validation, mar damages were created on a set of model amorphous polymethylmethacrylate (PMMA), polycarbonate (PC), and polystyrene (PS) samples following the ASTM-7027 standard, and their performance was assessed using a contrast-based approach. Meaningful correlation between FEM modeling and experimental results will be established. It is hoped that the present study can assist in the design of polymeric materials with improved mar visibility resistance.

## II. EXPERIMENTAL

### 1. Materials

The model amorphous polymers investigated in this study consist of commercialized PMMA (Plexiglas<sup>®</sup> V052), PC (Makrolon 2800), and PS (Polystyrol 158K) materials prepared using the injection molding process. Their melt flow rates and glass transition temperatures ( $T_g$ ) are presented in Table 1. Each system has dimensions of 150 mm × 150 mm × 3mm and 150 mm × 150 mm × 6mm for various mechanical characterization needs. PMMA samples were provided by Arkema Inc (King of Prussia, USA), while PC and PS samples were provided by BASF SE (Ludwigshafen, Germany). To obtain consistent mar results, all the samples have a high gloss piano black color and similar surface roughness.

Table 1. Melt flow rate and glass transition temperature ( $T_g$ ) of the model systems.

	Melt Flow Rate (cm <sup>3</sup> /10 min)	$T_g$ (°C)	( $R_a$ )
PMMA	2.4 (@ 230 °C, 3.8 kg)	116	36 ± 3 nm
PC	10 (@ 300 °C, 1.2 kg)	148	
PS	3.5 (@ 200 °C, 5 kg)	100	

## 2. Surface roughness embossing

The original surface roughness values of the model systems are  $(R_a)_{initial} = 36 \pm 3 \text{ nm}$ . It is difficult to investigate mar-induced ironing damage on such considerably smooth surfaces. Therefore, it is crucial to modify the surface roughness of the model samples in a consistent fashion without affecting their bulk properties. It has been found that embossing is a reliable process to achieve consistent nanometer to micrometer scale surface roughness in a repeatable fashion. Consequently, a stainless-steel plaque processed by electrical discharge machining (EDM) with a surface roughness of  $R_a = 3.24 \pm 0.07 \mu\text{m}$  was used to emboss similar surface roughness values on the model systems. The samples were compressed for 30 minutes using a PHI hydraulic press at a pressure of 1.3 MPa and a temperature  $10^\circ\text{C}$  above the  $T_g$  of the embossed polymer. The samples were then left to cool in the hot press until reaching at ambient temperature.

## 3. Surface roughness characterization

A Keyence VK9700 Violet Laser Scanning Confocal Microscope (VLSCM) was employed to measure the surface roughness of the embossed samples [23]. Measurements were taken on an embossing steel surface, the embossed model systems, and on the marred paths of the samples at distances of 10 (~15 N), 30 (~42 N), 50 (~75 N), 70 (~112 N), and 90 mm (~154 N) from the origin. At each location, measurements were conducted at five random nearby locations over an area of  $675 \times 506 \mu\text{m}$  using a 20x objective lens. A representative VLSCM image showing the roughness of embossed stainless steel is shown in Figure 1.

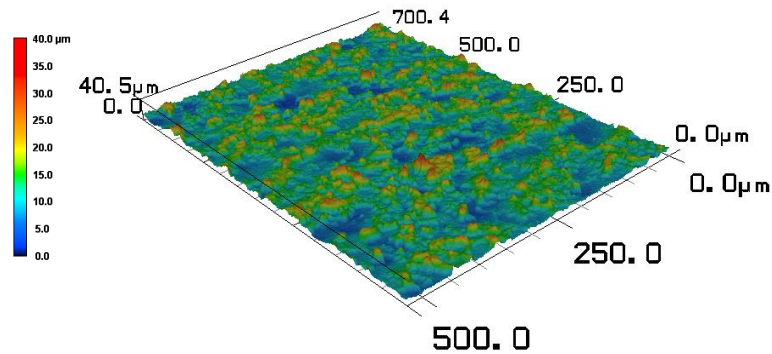


Figure 1. Representative VLSCM image of EDM-processed stainless steel plate.

## 4. Mar test

Mar tests were conducted according to ASTM D7027 / ISO 19252 standards [11, 24] using Scratch 5 Machine provided by Surface Machine Systems® (College Station, TX). Barrel mar tests were performed using a self-aligned stainless-steel barrel tip (Figure 2) with a length of 12 mm and a diameter of 10 mm. The test consists of applying a normal load linearly increasing from 1 to 180 N along the injection molding direction at a constant speed of 10 mm/s over a distance of 100 mm. To obtain consistent results, at least three mar tests were performed on each material. The

load range was chosen to allow for differentiation in mar visibility performance among the model systems.

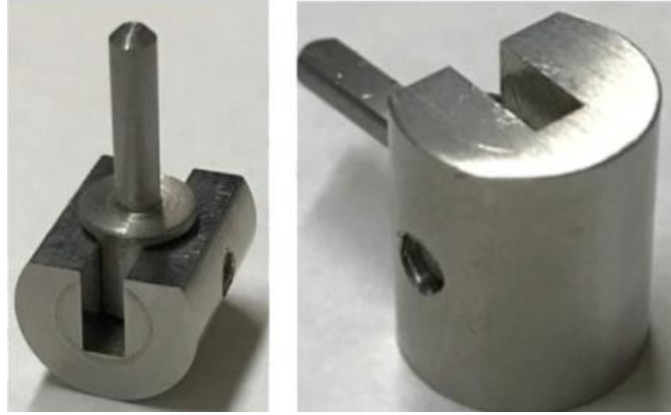


Figure 2. Self-aligned stainless-steel barrel tip used for mar test [1].

### 5. Coefficient of friction (COF)

The sample coefficients of friction (COF) of the embossed model polymer samples were determined by sliding a smooth stainless-steel flat tip with dimensions of  $10\text{ mm} \times 10\text{ mm}$  along the samples. A constant normal load of 3 N was applied over a distance of 100 mm at a speed of 10 mm/s. Five measurements were performed on each sample.

### 6. Mar visibility evaluation

The visibility of the marred samples were determined according to the procedure detailed in the previous study [1, 7, 25]. In short, samples were placed in a Black Box with dimensions of  $690\text{ mm} \times 430\text{ mm} \times 690\text{ mm}$  provided by Surface Machine Systems®. Preliminary tests showed that the observation angle should be set to  $90^\circ$  and the angle between the camera and the light source should be set to  $50^\circ$  to maximize the darkening effect caused by the ironing process. Then, mar images were analyzed using the Tribometric® software provided by Surface Machine Systems®. This software generates a curve showing the contrast value between the marred path and the virgin background of the sample as a function of the applied load. Figure 3 illustrates the areas utilized for mar visibility evaluation, which consist of a green box capturing the marred area and two surrounding white boxes indicating the background of the sample surface. The distance between the mar area and each of the background areas is 0.5 mm. At each pixel, the contrast value was determined using Equation (1):

$$\text{Contrast (\%)} = \frac{(I_m)^{1/\gamma} - (I_b)^{1/\gamma}}{(I_{max})^{1/\gamma}} \quad (1)$$

$I_m$  refers to the median brightness of the pixel line (blue area in Figure 3) in the mar path.  $I_b$  refers to the intensity of background, determined by the median grayscale value of two  $2\text{ mm} \times 0.5\text{ mm}$  areas in yellow boxes.  $I_{max}$  is the maximum captured intensity along the whole mar path.  $\gamma$  refers to the power-law scaling factor to normalize color intensity values.

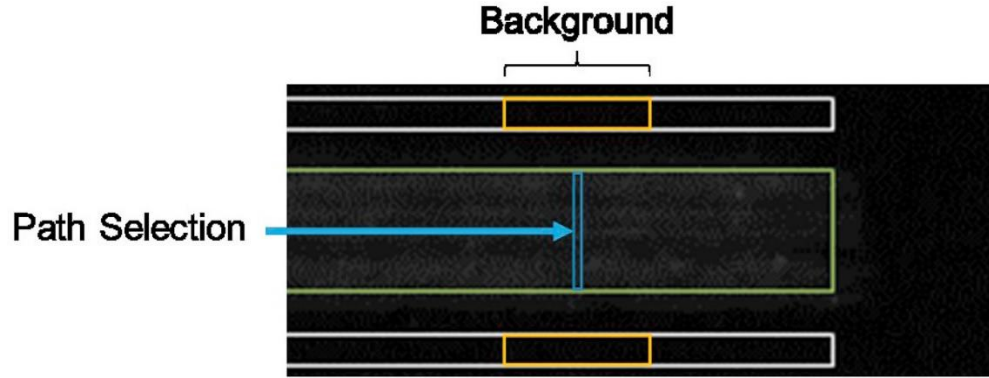


Figure 3. Areas utilized for mar visibility evaluation. [1]

## 7. Human observation procedure

Ten trained participants were involved in the human visibility assessment described previously [1, 26]. The test was conducted in a dark room to avoid background interference. Each of the participants was separately asked to rank the mar severity from 1 to 10, with 10 referring to the most visible mar. No information about the model system and testing conditions was given to the participants during the visibility assessment procedure.

## III. FEM MODELING

### 1. FEM model

The commercial finite element package ABAQUS 2017® was employed to perform the FEM modeling of the mar tests [27]. The dimensions and boundary conditions of the model are presented in Figure 4 [28, 29]. The mar tip was modeled as a rigid cylindrical body with an edge of 1 mm, and a spherical side with a diameter of 1 mm to suppress the stress singularities caused by the edge effect.

Eight-node 3D linear brick elements (C3D8R) with three nodal displacement degrees of freedom and reduced integration were considered to mesh the substrate. A refined mesh with element dimensions of  $46.5 \mu\text{m} \times 56.2 \mu\text{m} \times 30.0 \mu\text{m}$  was considered beneath the mar tip across a critical distance A-B for better computational performance and computational efficiency [30, 31]. Also, dynamic stress analysis and adaptive remeshing provided by ABAQUS were utilized in our model to preserve the mesh quality and avoid excessive distortion of the elements [8, 27].

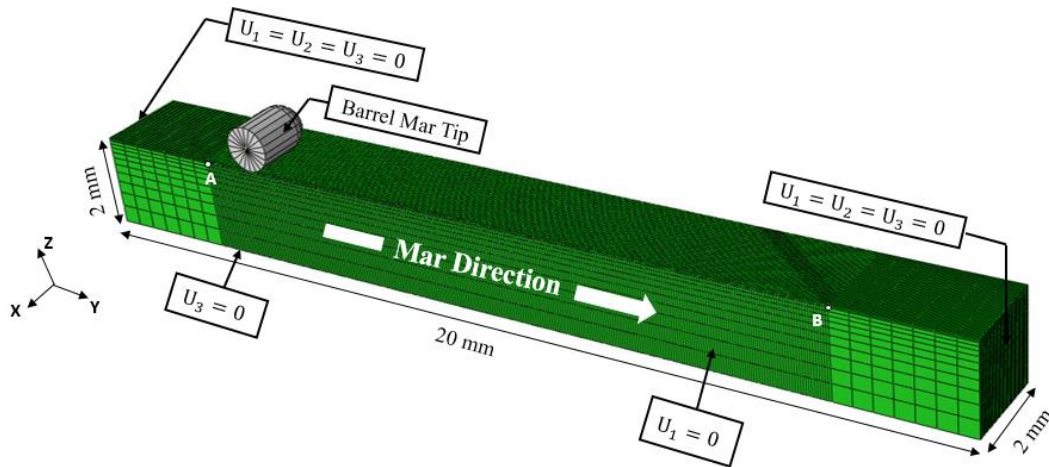


Figure 4. 3D finite element analysis model with the boundary conditions described.

## 2. Mar Simulation

The mar test was modeled in accordance with the same ASTM/ISO standards [11, 24]. For simplification purposes, the model did not consider node separation and element deletion after damage, heat generation, time and temperature-dependent response. The first step is the indentation test where the rigid mar tip moves down with an applied load of 0.5 N and comes into contact with the surface. Then, the mar process takes place and the tip slides over a distance of 12 mm with a speed of 10 m/s and a linearly increasing load from 0.5 to 50 N. The mar direction is indicated in Figure 4. A friction of  $\mu = 0.3$  was considered between the tip and the substrate. This is roughly the COF value of the roughened materials measured experimentally, as will be shown later. Finally, the tip stops at the end of the mar distance and moves upward allowing for material elastic recovery. The FEM modeling used in the present study including the constitutive model, boundary conditions, and mesh size has been validated by our previous single-path tribological studies [5, 15, 28].

## 3. Material properties

The 3D constitutive models, such as the Boyce-Parks-Argon (BPA) model [32-35] and the Eindhoven Glassy Polymer (EGP) model [18, 36-38], are shown to be capable of modeling the temperature and strain rate dependent intrinsic compressive behaviors of PC, PS and PMMA. However, to perform a meaningful parametric study and to identify the most relevant material parameters that affect mar behavior where the tensile behavior is also important, a simplified isotropic hardening model coupled with the experimentally obtained tensile and compressive true stress-strain curves were chosen to generate piece-wise linear curves for all the FEM modeling needs (Figure 5) [15]. These experimentally generated constitutive relations were found to be sufficient in capturing the mar behavior differences among the three model systems. Also, a previous work showed that the viscoelastic recovery of PC and SAN following the scratch test is limited and can be ignored [16]. In order to further simplify the simulation, PC, PMMA, and PS were assumed to be elastic-plastic materials without considering temperature and rate dependent

behavior. The main constitutive parameters are Young's modulus ( $E$ ), yield stress ( $\sigma_y$ ), softening slope ( $s$ ), and hardening slope ( $h$ ). The values of these parameters, as well as the density ( $\rho$ ), of the modeled materials are summarized in Table 2 [15].

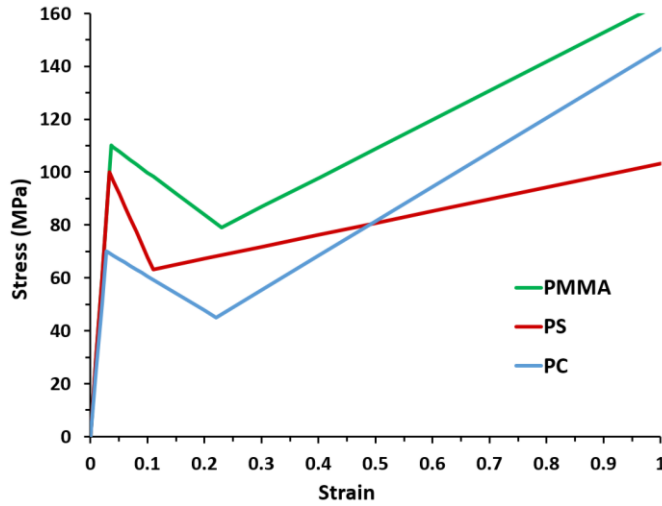


Figure 5. Typical piece-wise linear stress-strain curve of PMMA, PC and PS for FEM modeling.

Table 2. Constitutive parameters introduced in the FEM model.

Model System	$E$ (GPa)	$\sigma_y$ (MPa)	$s$ (MPa)	$h$ (MPa)	$\rho$ ( $g/cm^3$ )
PMMA	3	110	-160	110	1.18
PC	2.5	70	-130	130	1.20
PS	3	100	-480	45	1.04

#### 4. Parametric study

The impact of each of the constitutive parameters presented in Table 2 on the mar behavior is investigated separately by conducting a parametric analysis. Each of these parameters will be exclusively varied in the range of the model polymers investigated while maintaining the linear piece-wise stress-strain curves of the model systems. The values of the fixed and varying parameters for each case study are highlighted in Figure 6. It should be noted that the yield strain ( $\epsilon_y$ ) is slightly changed when altering elastic modulus or yield stress.

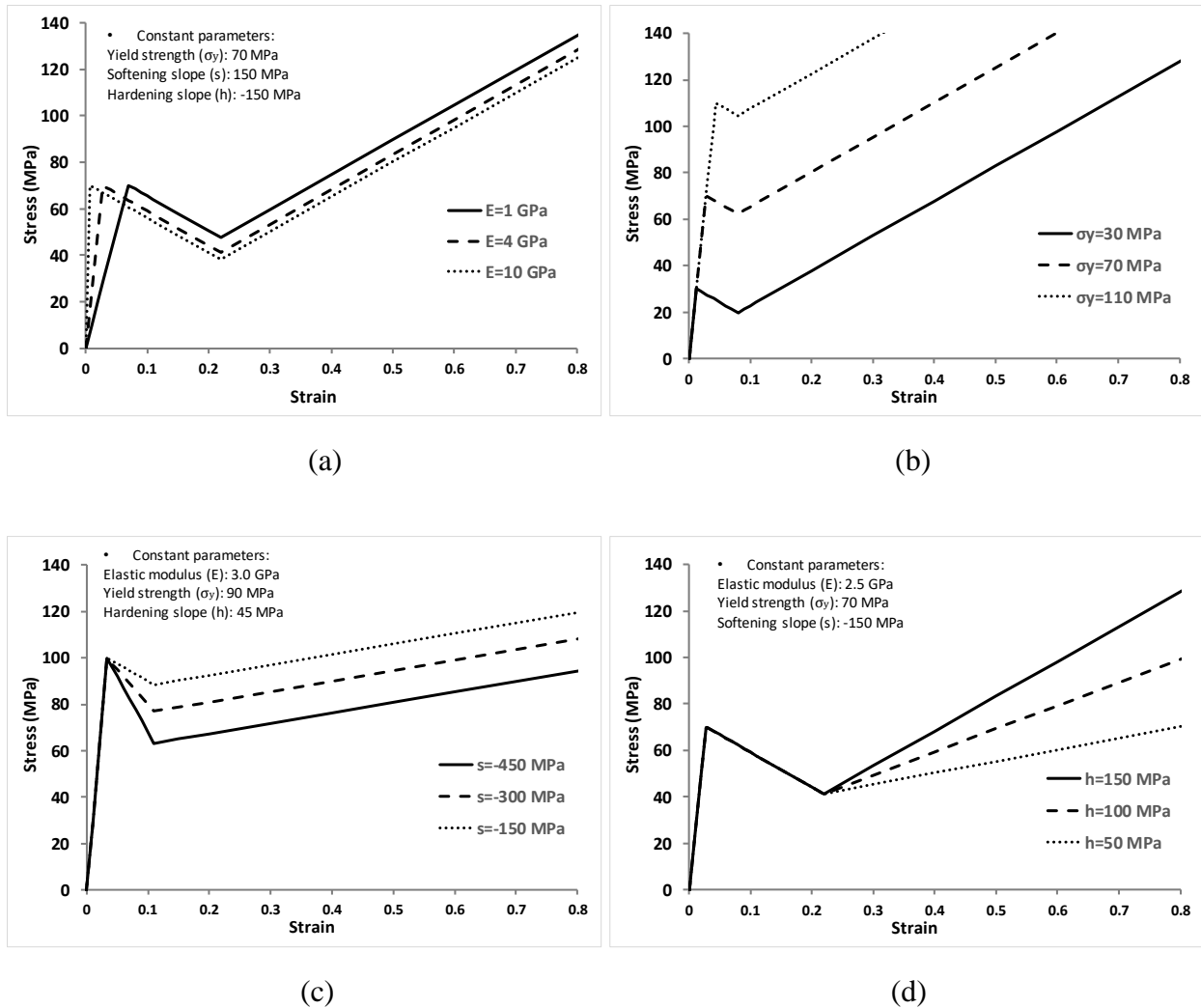


Figure 6. Fixed and varying constitutive parameters considered in the parametric study (a) elastic modulus (b) yield stress (c) strain softening slope, and (d) strain hardening slope.

## IV. RESULTS AND DISCUSSION

### 1. Experimental results

The surface coefficient of friction and root-mean-square (RMS) roughness ( $R_q$ ) of the examined model systems are presented in Figure 7. It is observed that the samples have similar COF and  $R_q$  values. Therefore, the difference in mar behavior to be discussed later will be mainly attributed to their respective constitutive behaviors, instead of to these two factors [39].

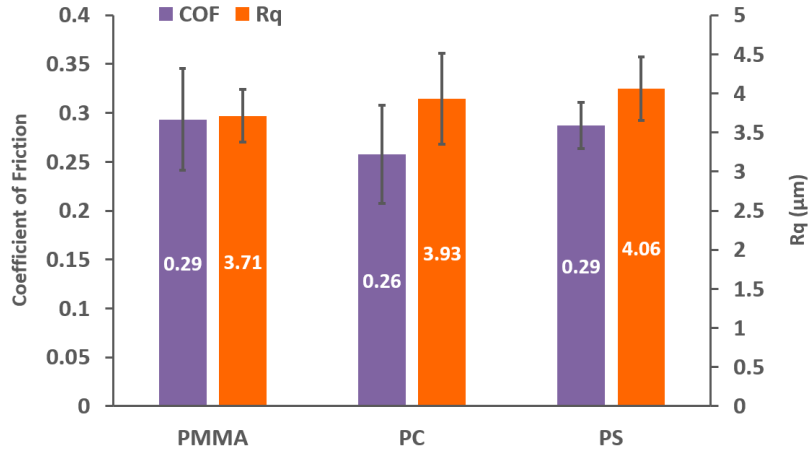


Figure 7. Surface coefficient of friction and roughness of the model systems.

Figure 8 presents the contrast curves along the mar path and the absolute integral area beneath them for each of the model systems. Figure 8a shows the representative contrast curves obtained by a moving average of 20 consecutive points to highlight the relative visibility. Also, the negative contrast values in this figure indicate the ironing effect due to the reduction in surface roughness, which causes mar damage to appear darker than the background [7, 40]. The contrast of the three model systems are indistinguishable below the 50 N mar load, suggesting no or extremely subtle mar damage was formed and cannot be resolved by the imaging tools utilized [41]. It was previously shown that the integrated area under the contrast curve is a straightforward way to quantify and compare the mar visibility resistance of polymers [39]. Higher integrated area is associated with lower mar visibility resistance. Figure 8b shows that PMMA has the lowest area beneath the contrast curve. Thus, this material is expected to have the highest mar visibility resistance. The integral area beneath the PC contrast curve is slightly smaller than that of the PS. This indicates that these two materials have similar mar visibility resistance, with PS having a lower mar resistance.

To validate their mar performance, the contrast-based findings presented above are compared with the human assessment results shown in Figure 9. The participants in the human assessment ranked mar damage on PMMA samples as the least visible, followed by that on PC which was ranked slightly lower than PS. These results are in agreement with the findings of the contrast analysis presented in Figure 8b.

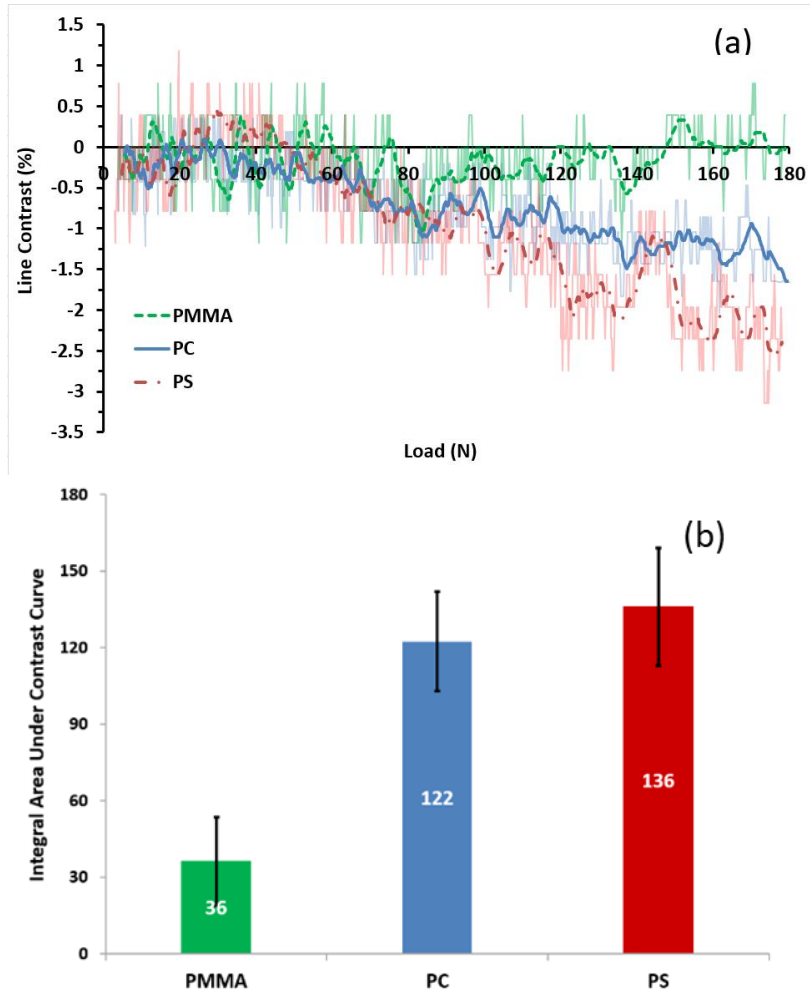


Figure 8. PMMA, PC, and PS (a) contrast curves and (b) absolute integral area under them.

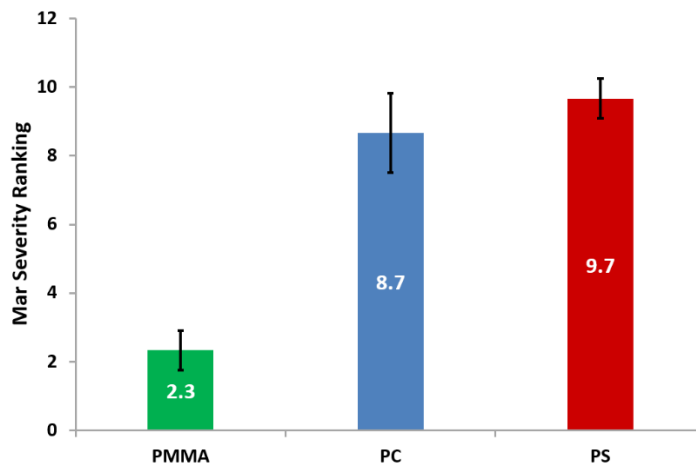


Figure 9. Ranking of mar visibility on the model systems.

As mentioned previously, no cracking or crazing damages were observed on the mar area. Therefore, the detected subtle mar damage is mainly associated with the surface roughness

changes. This effect can be studied using the percent change in surface roughness ( $\Delta R_q\%$ ) given by Equation (2):

$$\Delta R_q\% = \frac{R_q(\text{Marred}) - R_{q0}(\text{Virgin})}{R_{q0}(\text{Virgin})} \times 100\% \quad (2)$$

Figure 10 shows the values of  $\Delta R_q\%$  at different mar loads along the mar path. The negative value of this parameter signifies the ironing effect where the marred area is smoother than the background of the samples. A larger absolute  $\Delta R_q\%$  value demonstrates a more severe ironing effect due to the barrel mar process. As mentioned above, the severity of the ironing effect correlates well with visibility. The figure clearly shows that PMMA has the least absolute  $\Delta R_q\%$  value across the mar path which indicates its high mar visibility resistance. The two other materials, PC and PS, have similarly higher absolute  $\Delta R_q\%$  values reflecting their low mar resistance and large standard derivation. However, it should be noted that the average  $\Delta R_q\%$  value of PC is higher than that of PS below 55 N and the trend is reversed after that, probably due to the significantly higher strain hardening behavior of PC in the large-strain region [42]. These results are consistent with the contrast analysis shown in Figure 8 and the human assessment presented in Figure 9.

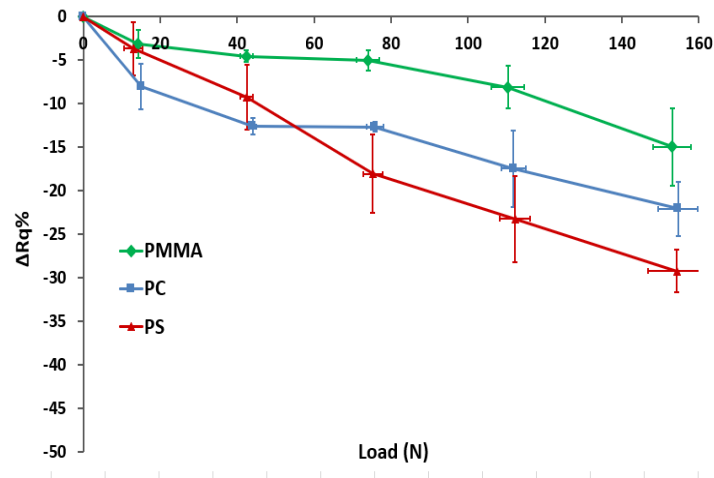


Figure 10. Difference in roughness between mar area and sample background along the mar path.

## 2. Finite Element Modeling

One of the major differences between mar simulation compared to scratch simulation is the presence of the edge effect in mar tests, which causes localized large-scale deformation. To avoid this effect, only the mid-section area within the mar path, i.e., the white dashed line region (0.8 mm × 11 mm) is considered (Figure 11). Since both the experimental and FEM simulation approaches have been validated in our previous studies [1, 5, 15, 28], the following analysis was conducted.

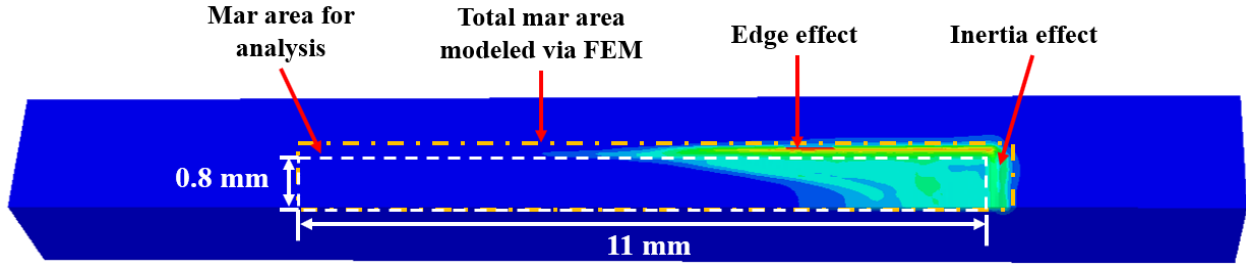
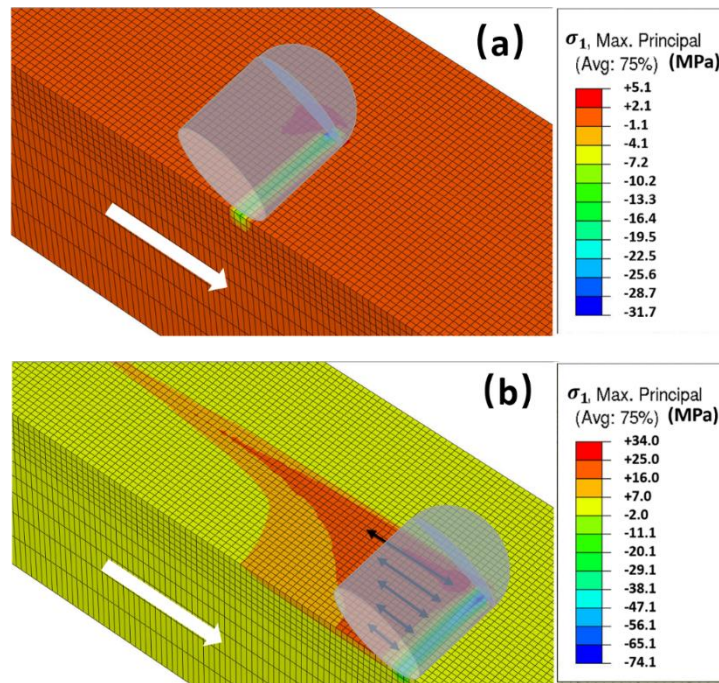


Figure 11. Considered area for mar analysis.

### a. Stress analysis

Due to the barrel tip and inertia effects, the stress distribution on mar surface is different than that in scratch [10, 31]. The distributions of maximum principal stress ( $\sigma_1$ ) on PC at different mar loads are shown in Figure 12. At a low mar load of 11 N, tensile and compressive stresses dominate at the edge and beneath the mar tip, respectively (Figure 12 a). As the applied normal load increases, the stress near the edge becomes more severe and high tensile stress is generated behind the mar tip (Figure 12 b, c), which is similar to previous scratch simulations [10]. This may indicate the formation of plastic yielding-related damage and meniscus wrinkling on the mar path.



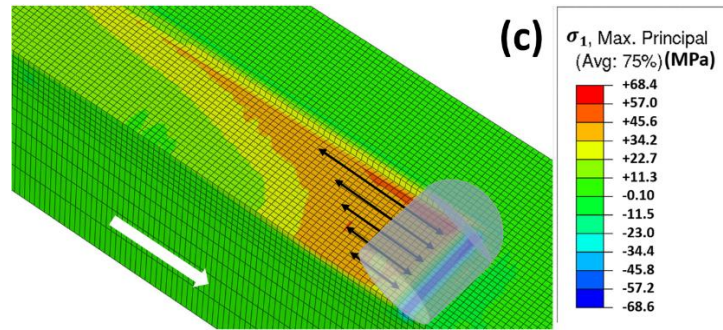
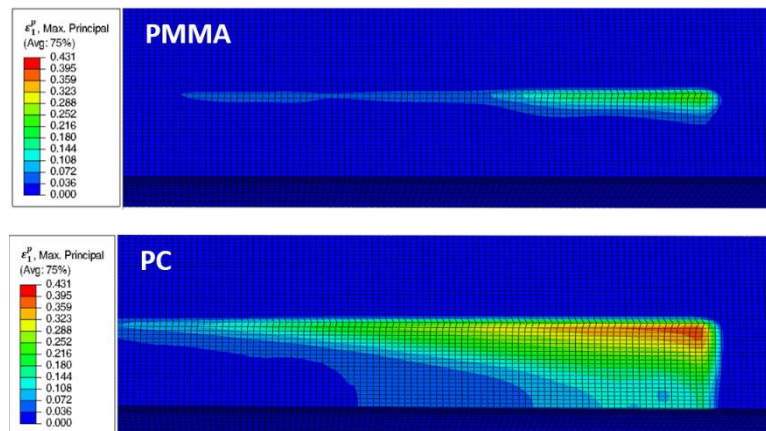


Figure 12. Maximum principal stress  $\sigma_1$  on PC at mar loads of (a) 11 N, (b) 34 N, and (c) 48 N.

The main objective of the FEM modeling is to conduct a parametric analysis that allows for the determination of the effect of different constitutive properties on mar resistance. However, it is crucial first to determine a parameter that can be used as a criterion to assess mar damage resistance. The parameters considered for this purpose are the maximum plastic principal strain ( $\epsilon_1^p$ ), maximum principal stress ( $\sigma_1$ ), von Mises stress ( $\sigma_v$ ), hydrostatic pressure ( $\sigma_p$ ), and total plastic energy dissipation ( $E_p$ ) [8, 43].

### b. Mar assessment criteria

*Maximum plastic principal strain ( $\epsilon_1^p$ ):* Figure 13 shows the distribution of  $\epsilon_1^p$  across the mar path of the three materials after the elastic recovery. The mar direction is from left to right. The figure shows that PMMA exhibits much lower  $\epsilon_1^p$  than PS and PC in terms of distribution and intensity. The magnitude of  $\epsilon_1^p$  is most significant in PS. These results are in agreement with the experimental (Figure 8) and human assessment findings (Figure 9). They indicate that  $\epsilon_1^p$  can be used as a criterion to assess mar damage resistance. This result can be explained by the mar-induced ironing effect being plastic deformation in nature, which makes the plastic principle strain a good criterion.



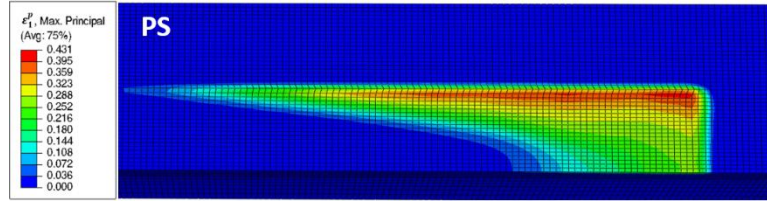


Figure 13. The contour plots of maximum plastic principal strain ( $\epsilon_1^p$ ) across the mar path of the modeled materials.

*Maximum principal stress ( $\sigma_1$ ):* Figure 14 shows the contours of  $\sigma_1$  across the mar path of the model polymers after the elastic recovery. The figure highlights that PMMA has the lowest  $\sigma_1$  level. However, it shows a higher  $\sigma_1$  intensity and magnitude on PC compared to PS. These results are inconsistent with the previous experimental findings and human assessment, showing that PC is ranked between PMMA and PS in terms of mar visibility resistance. Therefore, this parameter fails as a criterion for ranking mar damage resistance on the examined materials.

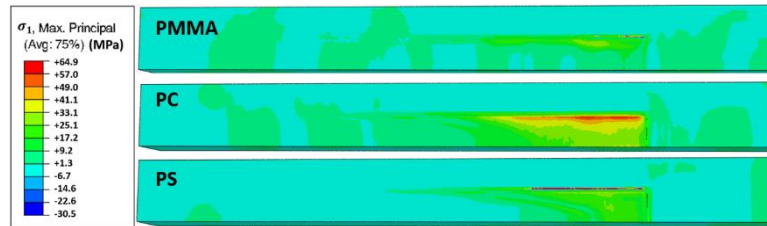
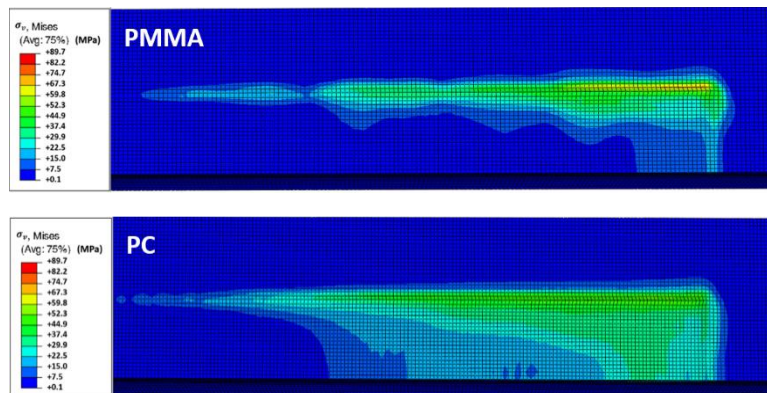


Figure 14. The contour plots of residual maximum principal stress ( $\sigma_1$ ) on the mar path of the modeled materials.

*von Mises stress ( $\sigma_v$ ):* Previous studies showed that von Mises stress was related to the onset of shear banding in polymers [44, 45]. Figure 15 highlights the  $\sigma_v$  contour plot across the mar path of the modeled materials. The figure shows that PMMA has the lowest values and PC exhibits higher values than PS, especially at the mar end. This parameter does not correlate well with the previous contrast-based analysis and human assessment. Therefore,  $\sigma_v$  fails as a criterion to reliably rank mar damage resistance on the examined samples. This finding suggests that the mar damage on the examined materials is not dominated by plastic yielding.



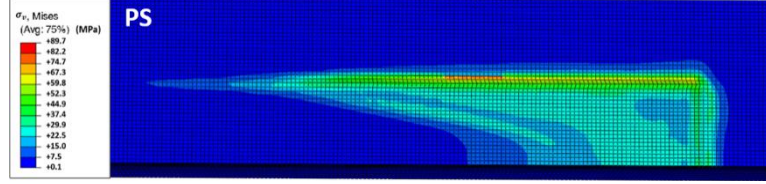


Figure 15. The contour plots of von Mises stress ( $\sigma_v$ ) on the mar path of the modeled materials.

*Hydrostatic pressure ( $\sigma_p$ ):*  $\sigma_p$  is known to be related to any damage mechanisms involving volume change, such as cracking, crazing, and voiding [46]. Figure 16 shows the contour plots on the surface of the model polymers. It is clearly shown that PMMA exhibits a much lower  $\sigma_p$  than PC and PS. The experimental and human assessment results show that PMMA has the best mar visibility resistance. This suggests that a lower hydrostatic pressure corresponds to a higher mar resistance. However,  $\sigma_p$  magnitude on PC is higher than that on PS which contradicts the experimental and human assessment findings. Therefore, the hydrostatic pressure fails as a criterion to assess the mar resistance of the examined samples. This suggests that mar damage on the tested materials is not dominated by mechanisms involving volume changes.

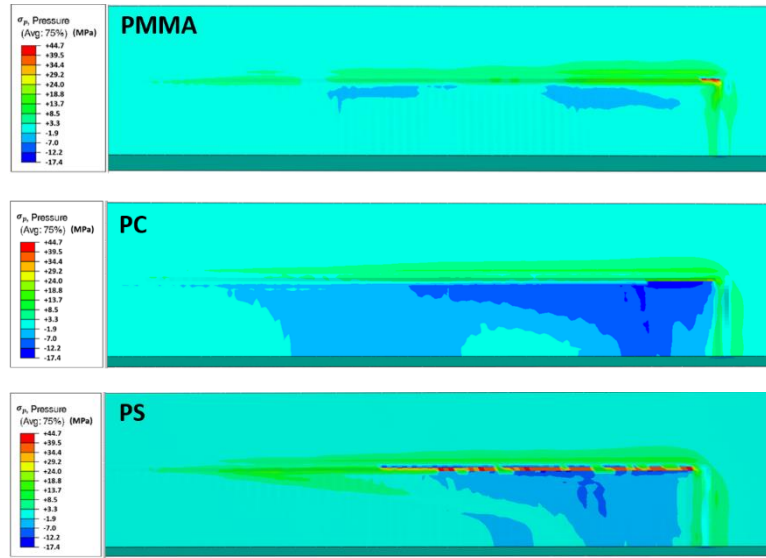


Figure 16. The contour plots of the hydrostatic pressure ( $\sigma_p$ ) on the mar path of the modeled materials.

*Total dissipated plastic energy ( $E_p$ ):* The energy conservation principle is highlighted by Equations (3) and (4) below. For simplicity, this principle does not consider temperature- and time-dependent deformations. It indicates that the kinetic energy ( $E_w$ ) on the mar tip is approximated by the summation of the dissipated frictional energy ( $E_f$ ) and the internal energy stored in the polymer substrate ( $E_I$ ) [27]. The barrel mar tip is modeled as an analytical rigid solid without internal energy. The value of  $E_I$  includes the elastic strain energy,  $E_s$ , and that dissipated by plastic mar deformation,  $E_p$ .

$$E_w \approx E_f + E_I \quad (3)$$

$$E_I = E_s + E_p \quad (4)$$

Figure 17 shows  $E_p$  values obtained from the mar area on PMMA, PC, and PS. It is found that PMMA has the lowest  $E_p$  value and that PC has slightly lower dissipated energy than PS. These results correlate well with the experimental findings (Figure 8) and human assessment (Figure 9). Therefore, the total dissipated plastic energy can be considered as a criterion to effectively evaluate the mar resistance of the studied materials.

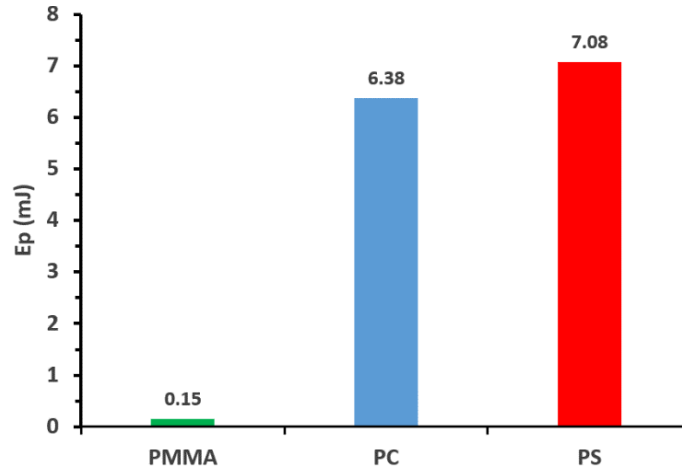


Figure 17. Total dissipated plastic energy ( $E_p$ ) of the modeled materials.

FEM results show that the maximum plastic principal strain ( $\epsilon_1^p$ ) and the total dissipated plastic energy ( $E_p$ ) are the most likely parameters that can be chosen to predict the mar visibility resistance of polymers. Higher mar resistance corresponds to lower  $\epsilon_1^p$  and  $E_p$  values. These two criteria will be used in the parametric study to determine how the constitutive properties influence mar visibility resistance of polymers [47].

### c. Parametric study

The parameters involved in the parametric analysis are elastic modulus ( $E$ ), yield stress ( $\sigma_y$ ), strain softening ( $s$ ), and strain hardening ( $h$ ). The surface COF is not included in this analysis because it has already been demonstrated that higher COF results in lower mar resistance [3, 13].

*Elastic modulus ( $E$ ):* Table 2 shows that the examined materials have similar elastic modulus values. Therefore, this property is not expected to affect the difference in their mar resistance. However, other materials may have significantly different modulus values and should be addressed. Figure 18 shows the effect of the elastic modulus on the maximum plastic principal strain and total dissipated plastic energy. It is found that a higher modulus leads to a higher  $\epsilon_1^p$  and higher  $E_p$  values, thus a lower mar resistance.

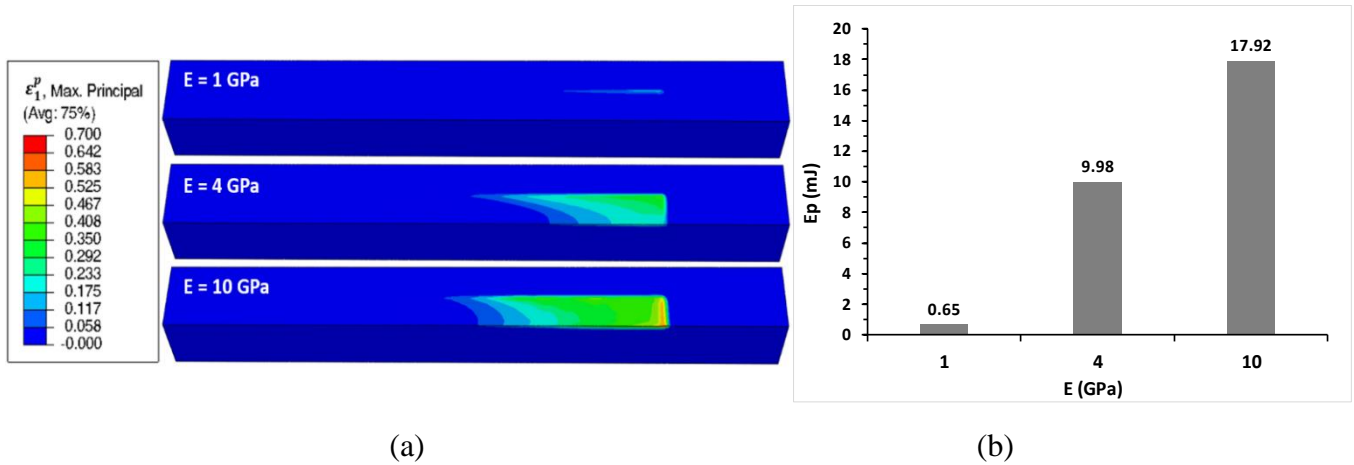


Figure 18. Effect of elastic modulus ( $E$ ) on (a) maximum plastic principal strain  $\epsilon_1^p$  distribution and (b) total dissipated plastic energy  $E_p$ .

*Yield stress ( $\sigma_y$ ):* Similarly, the impact of yield stress on  $\epsilon_1^p$  and  $E_p$  contour plots after recovery are presented in Figure 19. The figure shows that a higher yield stress corresponds to significantly lower  $\epsilon_1^p$  and  $E_p$  values. Since lower  $\epsilon_1^p$  and  $E_p$  values are associated with higher mar resistance, this result implies that a higher yield stress corresponds to a higher mar resistance.

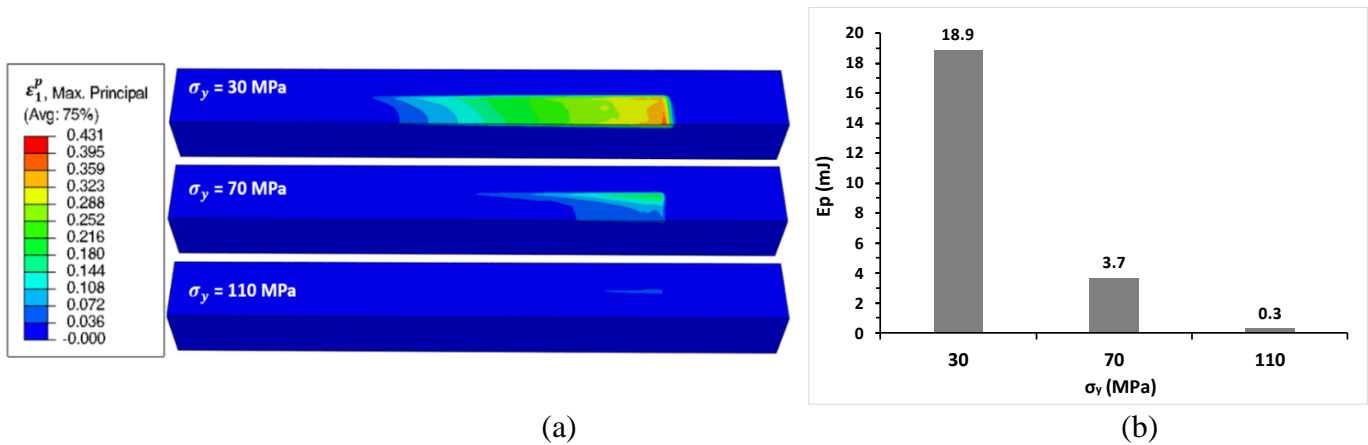


Figure 19. Effect of yield stress ( $\sigma_y$ ) on (a) maximum plastic principal strain  $\epsilon_1^p$  distribution and (b) total dissipated plastic energy  $E_p$ .

*Strain softening ( $s$ ):* Likewise, Figure 20 shows the effect of the strain softening slope on  $\epsilon_1^p$  and  $E_p$ . It is observed that a higher softening slope leads to higher  $\epsilon_1^p$  and  $E_p$  values. This suggests that higher slope corresponds to lower mar visibility resistance.

It is crucial to point out the impact of strain rate on strain softening. Strain softening is associated with localized inhomogeneous deformation, which makes it more dependent on the strain rate [38]. When the strain rate is slow enough, the strain softening phenomenon from uniaxial tensile or compression tests disappears [43]. Hence, the strain softening of amorphous

polymers measured by quasi-static uniaxial compression or tension tests may become more pronounced because of the much higher strain rate expected during the mar tests [13].

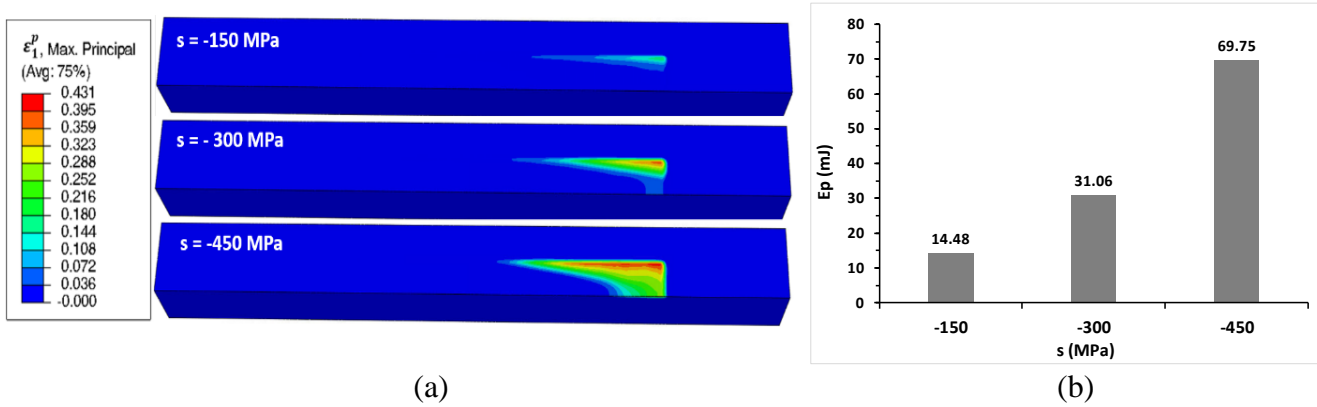


Figure 20. Effect of strain softening slope ( $s$ ) on (a) maximum plastic principal strain  $\epsilon_1^p$  distribution and (b) total dissipated plastic energy  $E_p$ .

*Strain hardening ( $h$ ):* Figure 21 highlights the effect of strain hardening slope ( $h$ ) on  $\epsilon_1^p$  and  $E_p$ . It is found that a higher strain hardening is associated with lower  $\epsilon_1^p$  and  $E_p$ , thus a higher mar resistance.

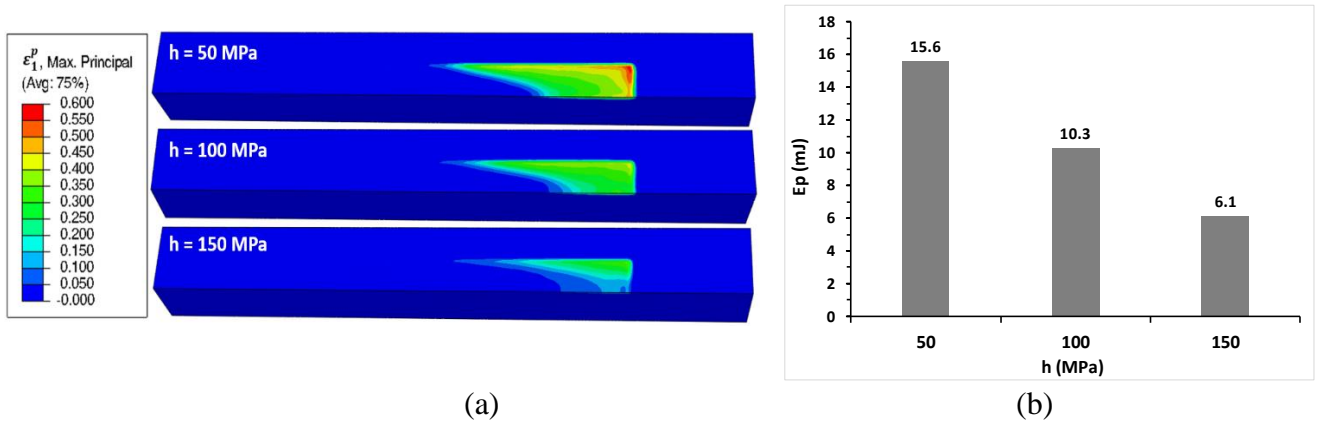


Figure 21. Effect of elastic modulus ( $h$ ) on (a) maximum plastic principal strain  $\epsilon_1^p$  distribution and (b) total dissipated plastic energy  $E_p$ .

Based on the above parametric analysis, the effect of the constitutive behavior on the mar resistance of PMMA, PC, and PS materials is summarized in Table 3. PMMA has the highest mar resistance because of its high yield stress, low strain softening slope, and high strain hardening slope. Although PC has a lower strain softening slope and a higher strain hardening slope, its mar resistance is compromised by its low yield stress. Finally, PS has a higher yield stress but a significantly higher strain softening slope and a lower strain hardening slope, which decreases its mar resistance considerably.

Table 3. Effect of the constitutive properties of the model systems on their mar resistance. Green = increased resistance, Red = decreased resistance.

	<b>Yield Stress</b>	<b>Softening Slope</b>	<b>Hardening Slope</b>
<b>PMMA</b>	<b>High</b> (110 MPa)	<b>Low</b> (-160 MPa)	<b>High</b> (110 MPa)
<b>PC</b>	<b>Low</b> (70 MPa)	<b>Low</b> (-130 MPa)	<b>High</b> (130 MPa)
<b>PS</b>	<b>High</b> (100 MPa)	<b>High</b> (-480 MPa)	<b>Low</b> (45 MPa)

The present study aims to investigate how the constitutive behaviors of polymers influence the mar visibility resistance. The model PMMA, PC, and PS were chosen to validate the framework of the FEM modeling. It is hoped that the present findings can serve as a guideline for the design of polymeric materials with improved mar visibility resistance. The FEM model developed in this study can be further improved in the future by considering the material's true stress-strain constitutive behavior, failure criteria, and viscoelastic behavior, which is the subject of our further research.

## V. CONCLUSION

The present study investigates the mar damage behavior of three model amorphous polymers: PMMA, PC, and PS. Mar tests were performed based on the ASTM D7027/ISO 19252 standards using a barrel mar tip. The experimental analysis shows that PMMA has minimal changes in surface roughness and contrast on the mar path against the virgin background of the sample. This indicates that PMMA has the best mar visibility resistance. To conduct a meaningful FEM parametric study, the criteria that can correlate well with the mar visibility resistance of the model polymers were determined to be the maximum principal strain and total plastic energy dissipation values. Results show that mar resistance improves with a lower elastic modulus, a lower strain softening slope, a higher yield stress, and a higher strain hardening slope. Future studies will include further validation on other polymeric systems.

## Acknowledgments

The authors would like to thank the financial support and valuable advice from Texas A&M Scratch Behavior Consortium members.

## References

- [1] J. Chrisman, S. Xiao, M. Hamdi, H. Pham, M. J. Mullins, and H.-J. Sue, Testing and evaluation of mar visibility resistance for polymer films, *Polymer Testing* 69 (2018) 238-244.
- [2] K. Friedrich, H. J. Sue, P. Liu, and A. A. Almajid, Scratch resistance of high performance polymers, *Tribology International* 44 (9) (2011) 1032-1046.
- [3] H. Pelletier, A. L. Durier, C. Gauthier, and R. Schirrer, Viscoelastic and elastic-plastic behaviors of amorphous polymeric surfaces during scratch, *Tribology International* 41 (11) (2008) 975-984.
- [4] L. C. A. van Breemen, L. E. Govaert, and H. E. H. Meijer, Scratching polycarbonate: A quantitative model, *Wear* 274 (2012) 238-247.
- [5] M. M. Hossain, R. Browning, R. Minkwitz, and H. J. Sue, Effect of Asymmetric Constitutive Behavior on Scratch-Induced Deformation of Polymers, *Tribology Letters* 47 (1) (2012) 113-122.
- [6] M. M. Hossain, R. Minkwitz, and H. J. Sue, Minimization of Surface Friction Effect on Scratch-Induced Deformation in Polymers, *Polymer Engineering and Science* 53 (7) (2013) 1405-1413.
- [7] H. Jiang, R. L. Browning, M. M. Hossain, H. J. Sue, and M. Fujiwara, Quantitative evaluation of scratch visibility resistance of polymers, *Applied Surface Science* 256 (21) (2010) 6324-6329.
- [8] M. Hamdi, X. Zhang, and H.-J. Sue, Fundamental understanding on scratch behavior of polymeric laminates, *Wear* 380-381 (2017) 203-216.
- [9] R. Browning, H. J. Sue, R. Minkwitz, and P. Charoensirisomboon, Effects of Acrylonitrile Content and Molecular Weight on the Scratch Behavior of Styrene-Acrylonitrile Random Copolymers, *Polymer Engineering and Science* 51 (11) (2011) 2282-2294.
- [10] H. Jiang, R. Browning, and H. J. Sue, Understanding of scratch-induced damage mechanisms in polymers, *Polymer* 50 (16) (2009) 4056-4065.
- [11] ASTM D7027-13 Standard Test Method for Evaluation of Scratch Resistance of Polymeric Coatings and Plastics Using an Instrumented Scratch Machine, 2013.
- [12] I. G. Goryacheva, *Contact Mechanics in Tribology*. Moscow: Kluwer Academic Publishers, 1998.
- [13] R. Browning, M. M. Hossain, J. Li, S. Jones, and H. J. Sue, Contrast-based evaluation of mar resistance of thermoplastic olefins, *Tribology International* 44 (9) (2011) 1024-1031.
- [14] J. W. S. Xiao, D. Lipka and H.-J. Sue, "Correlation of TAMU Scratch and Mar Test Methodology to Field Performance of Automotive Interior Parts," in *SPE Automotive TPO Engineering Polyolefin Global Conference Proceedings*, Troy, MI, 2017.
- [15] M. M. Hossain, H. Jiang, and H. J. Sue, Effect of constitutive behavior on scratch visibility resistance of polymers-A finite element method parametric study, *Wear* 270 (11-12) (2011) 751-759.
- [16] M. M. Hossain, R. Minkwitz, P. Charoensirisomboon, and H. J. Sue, Quantitative modeling of scratch-induced deformation in amorphous polymers, *Polymer* 55 (23) (2014) 6152-6166.
- [17] H. Pelletier, C. Gauthier, and R. Schirrer, Experimental and finite-element analysis of scratches on amorphous polymeric surfaces, *Mecanique & Industries* 9 (4) (2008) 261-271.
- [18] L. C. A. van Breemen, T. A. P. Engels, C. G. N. Pelletier, L. E. Govaert, and J. M. J. Den Toonder, Numerical simulation of flat-tip micro-indentation of glassy polymers: Influence of loading speed and thermodynamic state, *Philosophical Magazine* 89 (8) (2009) 677-696, Art. no. Pii 909461806.
- [19] W. J. Boo *et al.*, Morphology and mechanical behavior of exfoliated epoxy/alpha-zirconium phosphate nanocomposites, *Composites Science and Technology* 67 (2) (2007) 262-269.
- [20] P. Liu *et al.*, Influence of Trace Amount of Well-Dispersed Carbon Nanotubes on Structural Development and Tensile Properties of Polypropylene, *Macromolecules* 46 (2) (2013) 463-473.
- [21] S. V. Nair, S. C. Wong, and L. A. Goettler, Fracture resistance of polyblends and polyblend matrix composites .1. Unreinforced and fibre-reinforced nylon 6,6/ABS polyblends, *Journal of Materials Science* 32 (20) (1997) 5335-5346.
- [22] H. G. H. van Melick, L. E. Govaert, and H. E. H. Meijer, On the origin of strain hardening in glassy polymers, *Polymer* 44 (8) (2003) 2493-2502.

- [23] F. Lei *et al.*, Scratch behavior of epoxy coating containing self-assembled zirconium phosphate smectic layers, *Polymer* 112 (2017) 252-263.
- [24] ISO 19252:2008, *Plastics - Determination of Scratch Properties*, 2008.
- [25] M. Hamdi and H. J. Sue, Effect of color, gloss, and surface texture perception on scratch and mar visibility in polymers, *Materials & Design* 83 (2015) 528-535.
- [26] M. Hamdi, D. Manica, and H. J. Sue, A Multidimensional Scaling Analysis of Surface Perceptual Parameters on Scratch and Mar Visibility Resistance in Polymers, *Sae International Journal of Materials and Manufacturing* 10 (2) (2017) 94-106.
- [27] D. S. Corporation, *ABAQUS 2018 Documentation*, ed, 2018.
- [28] M. Hamdi, X. Zhang, and H.-J. J. W. Sue, Fundamental understanding on scratch behavior of polymeric laminates, 380 (2017) 203-216.
- [29] G. Molero, S. Du, M. Mamak, M. Agerton, M. M. Hossain, and H. J. Sue, Experimental and numerical determination of adhesive strength in semi-rigid multi-layer polymeric systems, *Polymer Testing* 75 (2019) 85-92.
- [30] M. M. Hossain, "Quantitative modeling of polymer scratch behavior," Doctor of Philosophy, Texas A&M University, 2013.
- [31] G. T. Lim, "Scratch behavior of polymers," Texas A&M University, 2005.
- [32] E. M. Arruda and M. C. Boyce, Evolution of plastic anisotropy in amorphous polymers during finite straining, *International Journal of Plasticity* 9 (6) (1993) 697-720.
- [33] M. C. Boyce and E. M. Arruda, An experimental and analytical investigation of the large strain compressive and tensile response of glassy polymers, *Polymer Engineering and Science* 30 (20) (1990) 1288-1298.
- [34] M. C. Boyce, D. M. Parks, and A. S. Argon, Large inelastic deformation of glassy-polymers .1. Rate dependent constitutive model, *Mechanics of Materials* 7 (1) (1988) 15-33.
- [35] W. M. Gao, L. Wang, J. K. Coffey, and F. Daver, Understanding the scratch behaviour of polymeric materials with surface texture, *Materials & Design* 146 (2018) 38-48.
- [36] L. E. Govaert, P. H. M. Timmermans, and W. A. M. Brekelmans, The influence of intrinsic strain softening on strain localization in polycarbonate: Modeling and experimental validation, *Journal of Engineering Materials and Technology-Transactions of the Asme* 122 (2) (2000) 177-185.
- [37] E. T. J. Klompen, T. A. P. Engels, L. E. Govaert, and H. E. H. Meijer, Modeling of the postyield response of glassy polymers: Influence of thermomechanical history, *Macromolecules* 38 (16) (2005) 6997-7008.
- [38] L. C. A. van Breemen, T. A. P. Engels, E. T. J. Klompen, D. J. A. Senden, and L. E. Govaert, Rate- and temperature-dependent strain softening in solid polymers, *Journal of Polymer Science Part B-Polymer Physics* 50 (24) (2012) 1757-1771.
- [39] M. Hamdi and H.-J. Sue, Effect of color, gloss, and surface texture perception on scratch and mar visibility in polymers, *Materials & Design* 83 (2015) 528-535.
- [40] M. Hamdi, "Fundamental Understanding of Scratch and Mar Behavior of Polymers," Doctoral dissertation, Department of Mechanical Engineering, Texas A&M University, 2016.
- [41] H. Pelletier, C. Gauthier, and R. J. T. I. Schirrer, Relationship between contact geometry and average plastic strain during scratch tests on amorphous polymers, 43 (4) (2010) 796-809.
- [42] D. J. A. Senden, S. Krop, J. A. W. van Dommelen, and L. E. Govaert, Rate- and temperature-dependent strain hardening of polycarbonate, *Journal of Polymer Science Part B-Polymer Physics* 50 (24) (2012) 1680-1693.
- [43] Narisawa. I, A. F. Yee, and J. P. Harcup, *Strength, Fracture and Fatigue of Polymers*, Elsevier (2006).
- [44] S. Abrate, Criteria for yielding or failure of cellular materials, *Journal of Sandwich Structures & Materials* 10 (1) (2008) 5-51.
- [45] D. C. Drucker and W. Prager, Soil mechanics and plastic analysis for limit design, *Quarterly of Applied Mathematics* 10 (2) (1952) 157-165.

- [46] S. S. Sternstein, Flaws, Anisotropy and failure of solid polymers, *Journal of Rheology* 23 (3) (1979) 412-413.
- [47] M. Hamdi, M. Puopolo, H. Pham, and H.-J. Sue, Experimental and FEM analysis of scratch behavior on polypropylene thin films: Effect of film orientation and ethylene monomer content, *Tribology International* 103 (2016) 412-422.